Co-Doped mesoporous titania photocatalysts prepared from a peroxo-titanium complex solution

Ibrahim El Saliby[a], Laszlo Erdei[b], Andrew McDonagh[c], Jong-Beom Kim[d,e], Jong-Ho Kim[d,e], and Ho Kyong Shon[a]*

[a] Faculty of Engineering and Information Technology, University of Technology Sydney, NSW 2007, Australia

[b] Faculty of Engineering and Surveying, University of Southern Queensland, QLD 4350, Toowoomba, Australia

[c] Faculty of Science, University of Technology Sydney, NSW 2007, Australia

[d] The Research Institute for Catalysis, Chonnam National University, Gwangju 500-757, South Korea

[e] Photo & Environmental Technology Co. Ltd., Gwangju 500-460, South Korea

*Corresponding author email: hokyong.shon-1@uts.edu.au, Phone: +61 2 9514 2629, fax: +61 2 9514 2633

Abstract

In this study, nitrogen doped and nitrogen/silver co-doped TiO_2 photocatalsysts were fabricated using a sol-gel method at room temperature. The obtained gels were neutralised, washed with pure water, and calcined at 400 °C for 4 hours. The photocatalysts were characterised by scanning and transmission electron microscopy, X-ray diffraction, diffuse reflectance spectroscopy, X-ray photoelectron spectroscopy, and BET specific surface area.

The results showed that spherical particles with anatase structure were produced after annealing at 400 °C. N 1s (400 eV) and Ag 3d (367.3 eV) states indicated that nitrogen doping and silver co-doping were in the form of NO bonds and AgO, respectively. The photocatalytic activity of photocatalysts was investigated using a batch reactor system exposed to artificial solar irradiation. Both nitrogen and silver/nitrogen co-doped materials were effective in the photocatalytic degradation of hexamethyl pararosaniline chloride.

Keywords: TiO_2, solar light, photocatalysis, co-doping, crystal violet.

1. Introduction

Recent advances in material synthesis have combined the development of interesting microstructures and nanoassemblies with environmental applications such as water purification. Investigations into photocatalytic reactions with doped TiO_2 have shown enhanced reactivity under visible light irradiation compared with undoped TiO_2 [1-3]. Sato et al. [1] were the first to describe the synthesis of nitrogen-doped TiO_2 obtained by calcination of titanium hydroxide. The authors confirmed that nitrogen was acquired from NH_4OH, which was used in the hydrolysis of $TiCl_4$ to prepare titanium hydroxide. Asashi et al. [2] reported that substitutional doping using several non-metal elements promotes the visible light reactivity of TiO_2. Moreover, they stated that nitrogen doping was the most effective because a band-gap narrowing was attained by mixing the *p* states of N with O 2*p* states. Consequently, many research groups [4-12] have reported theoretical and experimental studies on promising methods to produce visible-light sensitive TiO_2 photocatalysts. Burda et al. [4] noticed that the direct amination of TiO_2 changed the original whitish colour to yellow. The incorporation of N into the TiO_2 cluster has been achieved by a number of methods. Ammonolysis, wet chemical route and modified peroxide sol-gel method have been reported by Michalow et al. [7], Bianchi et al. [13] and Jagadale et al. [6], respectively. Generally, the use of aqueous ammonia for the preparation of peroxotitanate complexes and TiO_2 nanomaterials is used [6, 14-17]. Nevertheless, previous work mainly focused on changes in morphology and crystal phase of TiO_2 rather than on N doping.

Metal co-dopants such as W, V and Ag can further enhance the photocatalytic reactivity of TiO_2 nanopowders [18-20]. The preparation of nitrogen and silver co-doped nanomaterials using a peroxide method was achieved by soaking TiO_2 in a solution of H_2O_2 and NH_4OH [20]. The obtained nanopowders showed reactivity under visible light for the photodegradation of methylene blue. Multidimensional nanoassemblies and microstructures

have also been examined including high-performance Ag/TiO_2 nanofiber membranes [23], nitrogen-doped flower-like ZnO materials [24] and the self-etching reconstruction of mesoporous $F\text{-}TiO_2$ hollow microspheres [25].

Many dye wastewaters represent threat to the environment, by colouring natural water and destabilising the equilibrium of ecosystems. Several ways could be used to treat dye wastewaters, for instance, heterogeneous photocatalysis is an effective technology for decomposing cytotoxic and carcinogenic dyes into harmless inorganic compounds. Crystal violet (CV) has been previously used as a model organic pollutant to test the efficiency of photocatalytic systems [21-22]. The photodegradation pathways of CV were reported [22] and occur in several steps: at the beginning, the generation of many N-demethylated intermediates is predominant, then, pararosaniline is formed as a final dye, at the end, several mineralisation reactions of organic by-products (formic acid, oxalic and acetic acids) take place.

Here, we report a novel peroxide method for the preparation of mesoporous photocatalysts doped with silver and nitrogen. The incorporation of dopants was achieved by the dissolution and precipitation of TiO_2 nanopowder (Evonik P25) at room temperature. The doped products were characterised for morphological and chemical changes and their photocatalytic activity was tested for the photodegradation of crystal violet under solar light.

2. Experimental

2.1 Materials

Aeroxide® TiO_2 (Degussa Evonik P25), which is comprised of a mixture of anatase, rutile and amorphous structures, with a mean surface area (BET) of 50 m^2/g, was used as received. Ammonium hydroxide (25% w/w) was purchased from Fluka (Sigma-Aldrich, Germany); silver nitrate (99.5%) was obtained from Fluka (Sigma-Aldrich, UK), and hydrogen peroxide

(50%, ACR laboratory reagent) from Australian Scientific. Nitric acid (69.5%, reagent grade, Scharlau chemie S.A) and hydrochloric acid (37%, reagent grade, Scharlau chemie S.A) were used for pH adjustment. CV (88% purity) was acquired from Chem-supply Pty Ltd (South Australia, Australia). Ultrapure (Milli-Q) water was used to prepare solutions.

2.2 Synthesis of photocatalysts

Nitrogen-doped TiO_2 nanoparticles were prepared by dissolving 1 g of TiO_2 powder in a mixture of 10 ml of ammonium hydroxide and 20 ml of hydrogen peroxide in a Teflon cell at room temperature (Figure 1). The mixture was neutralised with 1 N HCl, washed with Milli-Q water and separated from the suspension by centrifugation (Centurion Sci., 2040) at 3000 rpm for 5 min. Silver co-doping was accomplished by dissolving the desired amount of $AgNO_3$ in solution C (Figure 1). However, HNO_3 was used instead of HCl in the neutralisation step to avoid the precipitation of silver chloride. The obtained nanomaterials were dried in oven at 100 °C for 12 h and then calcined at 400 °C for 4 h. Nitrogen-doped and silver co-doped photocatalysts are expressed hereafter as TiN and TiNAg, respectively.

2.3 Characterisation of photocatalysts

The surface area and pore structure of photocatalysts were examined by means of nitrogen (N_2) adsorption-desorption analyses using the BET and BJH methods. Nitrogen physical adsorption was performed using an automated surface area analyser (Micromeritics Gemini 2360, USA). Scanning electron microscope (SEM) micrographs were obtained by a FEI XL30 ESEM operating at 25 kV. High magnification images were obtained from a Philips CM200 (Netherland) transmission electron microscope (TEM) operating at 200 kV. XRD powder diffraction patterns were generated on a MDI Jade 5.0 (MaterialsData Inc., USA) X-ray diffractometer with Cu Kα radiation source. The data were measured within the scattering

angle 2θ range of 5º-85º. Nitrogen and silver content and chemical states were measured using a Multilab2000 (VG, UK) X-ray photoelectron spectra (XPS) instrument with a non-monochromatic Mg Kα radiation at a residual gas pressure of below 10^{-9} Pa. Diffuse reflectance spectra of powders were measured on a UV–vis scanning spectrophotometer (Cary 500 Scan, Varian, USA) by placing a thin film in the sample holder, which was inserted in the integrated sphere for reflectance measurements between 300 nm and 700 nm.

2.4 Photocatalytic activity

The photocatalytic activity of nanopowders was studied by decomposing CV under simulated solar light. Batch experiments were carried out in glass beakers containing 200 mL of 10 mg/L CV solution (pH = 6.2). After the addition of the desired amount of photocatalyst (1 g/L), the suspension was mixed with a magnetic stirrer at 360 rpm for 30 min (dark adsorption). After reaching the adsorption equilibrium, photocatalysis took place in a Solar simulator (SolSim v1.2, Luzchem Research Inc., Canada) equipped with a 300 W Xenon lamp, a temperature controller, a magnetic stirrer and an air sparger to provide dissolved oxygen. Photocatalysis was carried out at 50,000 lx of simulated solar light for 6 h at a stable temperature of 26 ºC. Slurry samples were collected at fixed time intervals, filtered through 0.45 µm Teflon syringe filters (Whatman, UNIFLO) and analysed using a Shimadzu UV-Vis 1700 spectrophotometer and a Multi N/C 3100 (Analytik Jena) dissolved organic carbon (DOC) analyser. The decrease in CV concentration was assessed by the decrease in the absorbance band at 590 nm over time.

Standard CV solutions were prepared and their absorbance was measured to draw a mathematical relationship between the decrease in absorbance and CV concentration. The linear relationship generated had the following formula:

Abs (cm^{-1}) = 0.018 + 0.166*$[CV]$

R^2 = 0.997

where Abs is the absorbance at λ = 590 nm and $[CV]$ is the concentration of dye in mg/L.

3. Results and discussion

Morphology and porosity

Figure 2 shows SEM images of TiN and TiNAg powders. A mixed morphology of isotropic microspheres and aggregated nanoparticles is observed. The typical grain morphology of TiN and TiNAg is relatively similar with the majority of spheres in the size range of 1 to 2 μm. In TiNAg samples, silver could be detected by Ag flaring, revealing the scattered distribution of Ag on the TiO_2 surface.

High magnification TEM images (Figure 3) revealed that the microspheres were composed of a large number of nanoparticles aggregated in a spherical form. Both photocatalysts showed a disordered mesostructure with a wide pore size distribution. Mesopores (2-50 nm) were formed among large nanoparticles (20-70 nm in size) in TiNAg, and in between smaller nanoparticles (5-40 nm in size) in TiN.

XRD analysis of diffraction patterns indicated that both TiN and TiNAg have the anatase crystal structure (Figure 4). Peaks at 2θ diffraction angles equal to 25.2°, 38°, 48.2°, 55° and 62.5° were detected, which are attributed to different diffraction planes of anatase TiO_2. Silver diffraction peaks were absent in the XRD patterns due to the low Ag concentration and scattered distribution on the surface of TiO_2.

Important physical parameters of the photocatalysts are summarised in Table 1. The as-prepared powders (before calcination at 400 °C for 4 h) showed a large surface area, up to

383.4 m^2/g and 399.38 m^2/g for TiN and TiNAg, respectively, but were reduced significantly by the calcination process. BET surface areas of calcined samples were comparable being 52.47 m^2/g and 52.91 m^2/g for TiN and TiNAg, respectively. Mean mesopore diameters (BJH desorption data) of TiN and TiNAg were 4.63 nm and 6.08 nm, respectively. Nitrogen adsorption/desorption isotherms are shown in Figure 5. The adsorption isotherms have hysteresis loops that started at low N_2 relative pressure owing to mesoporous characteristics. The isotherm curves were of type IV with H3 hysteresis loop that is usually observed with aggregates of plate-like particles leading to slit-shaped pores [26].

3.1 DRS analysis

Figure 6 shows the DRS spectra of the prepared samples. The absorbance properties of TiN and TiNAg were significantly different to those of undoped TiO_2. The absorbance spectrum of the N-doped sample calcined at 400 °C showed absorption at longer wavelengths than that of P25 [27]. Figure 6 also revealed an important band gap narrowing of the TiN photocatalyst compared to P25. The combination of N and Ag further shifted the absorbance to longer wavelengths but reduced the absorbance at all wavelengths. While TiN displayed the typical shoulder at ~450 nm associated with localised electronic states near the conduction band [28], TiNAg exhibited a continuous shift to 550 nm.

3.2 XPS analysis

Figure 7 shows the XPS spectra in the N 1s and Ag 3d regions for TiN and TiNAg. For TiN, O 1s peaks were recorded at 530.1 eV and 531.4 eV and were ascribed to O-Ti-O oxygen coordination and chemisorbed oxygen or hydroxyl oxygen atoms, respectively [6]. The N 1s peak at 400.1 eV indicated that N exists in the form of adsorbed NO [1, 5, 27, 28]. The assignment of the N 1s peak has been a source of debate for researchers in the past few years.

Peak assignment in nitrogen doped TiO_2 has been reviewed and discussed in detail by Emeline and co-workers [28]. Sato et al. [1] reported the synthesis of N-doped TiO_2 by a wet method and their XPS results showed an N 1s peak at 400 eV, which was assigned to adsorbed NO_x species. In our case, nitrogen incorporation appeared in the form of Ti-O-N, based on the binding energies of O (≈ 530 eV and 531.4 eV) and N (≈ 400 eV). Before the calcination of TiN powder at 400 °C, two distinct N 1s peaks were detected at approx. 400 eV and 405 eV, at 5 at.% N content and the samples had a strong yellow colour. After calcination, the peak at 405 eV disappeared from the spectrum, the nitrogen content was reduced to 1.38 at.% and the colour became pale yellow (Table 2). These changes indicated that most of the adsorbed nitrogen species (mainly NO_x) were desorbed during annealing.

In the TiNAg sample, similar nitrogen (≈ 399 eV) and oxygen (≈ 530 eV) peaks were recorded (O-Ti-O, N-O-Ti). The percentage of N was higher in co-doped samples, while the Ag content ranged from 0.15 at.% to 0.2 at.% (Table 2). Gu et al. [18] also found that the concentration of N in N-doped samples was lower than in N-V co-doped powders, ascribing this to the decrease in the energy barrier for nitridation caused by V atoms. Ag 3d peaks indicated that silver exists in Ag^{3+} or AgO forms [22, 29]. Since the ionic radius of Ag^{+} (129 pm) is significantly bigger than that of Ti^{4+} (74.5 pm), physical substitution is unlikely to occur. However, Ag^{3+} (89 pm) and Ti^{3+} (81 pm) have relatively similar ionic radii, which increased the chance of substitution between the two. This was further substantiated by the binding energies of Ag 3d5 (365.8 eV) and Ti 2p3 (457.8 eV). The lattice distortion caused by the incorporation of Ag in TiO_2 induced a decrease in the bond strength of O-Ti-O bonds [30]. In turn, this reduced the energy barrier and allowed for more N atoms to bind to O in the form of NO species.

3.3 Photocatalytic activity

The photocatalytic degradation of Crystal Violet (CV) over time is shown in Figure 8. The decrease of absorbance at $\lambda = 590$ nm due to photolysis (in the absence of photocatalyst) was insignificant, about 10-15% in 6 h of simulated solar light irradiation. However, this discolouration (photo-bleaching) was not coupled with a decrease in dissolved organic carbon (DOC), which indicated the degradation of CV into several N-de-methylated reaction intermediates (organic by-products) [31].

After the addition of photocatalyst, the suspension was left in dark for 30 min to reach adsorption equilibrium. Both photocatalysts showed low adsorption affinity to CV, decreasing the concentration of dye in solution by approx. 5%. The discolouration of CV solution was almost complete after 6 h of irradiation. Little difference was observed between TiN and TiNAg for the discolouration of CV under the experimental conditions described above. The limited increase in photocatalytic activity for the co-doped photocatalysts may be due to the relatively low concentration and scattered distribution of Ag.

It should be noted that the decrease in colour only indicated the photo-bleaching of dyes but not their complete mineralisation in photocatalytic reactions. However, photocatalytic mineralisation can be verified by measuring the decrease of DOC during photocatalysis. DOC results shown in Figure 8 indicated that the photodegradation of organic by-products was not complete after 6 h of photocatalysis. DOC was decreased from 6.3 mg/L to 2.8 mg/L and 2.5 mg/L for TiN and TiNAg, respectively. The results showed that TiN and TiNAg had comparable performances in the photo-mineralisation of CV and its N-de-methylated by-products. Furthermore, data on absorbance at $\lambda = 540$ nm (pararosaniline detection wavelength) indicated no residual colour at the end of the experiment (Figure 8). The photodegradation of pararosaniline was investigated by Martins et al. [32]. The analysis of formed by-products by the degradation process showed that formic acid is the main organic compound present in solution in addition to carboxylic acid, aldehydes and ketones. In our

case, the residual DOC revealed the persistence of organic by-products in solution which needed more time for complete mineralisation. These by-products would be a mixture of formic acid, carboxylic acids, aldehyde and ketones. Their total removal is possible by prolonging the photodegradation reaction time.

4. Conclusions

The synthesis of N doped and N/Ag co-doped photocatalysts was done using a simple sol-gel method at room temperature. TiN and TiNAg showed mixed morphology of aggregated nanoparticles and spherical microspheres. The obtained amorphous powders were crystallised to anatase forms after annealing at 400 °C for 4 h. Both materials revealed N 1s peak around 400 eV which can be assigned to NO adsorbed species. The Ag doping state was identified in the form of Ag^{3+} or AgO. Both photocatalysts were able to decolourise and reduce the DOC of CV solutions under simulated solar light irradiation.

Acknowledgment

This research was funded by ARC-LP (LP0991544), a UTS internal grant and Australian Postgraduate Award scholarship. This work was also supported by Priority Research Centers Program through the National Research Foundation of Korea (NRF) funded by the Ministry of Education, Science and Technology (2011-0030747).

References

[1] S. Sato, Chem. Phys. Lett. 123 (1986) 126-128.

[2] R. Asahi, T. Morikawa, T. Ohwaki, K. Aoki, Y. Taga, Science 293 (2001) 269-271.

[3] E. Stathatos, T. Petrova, P. Lianos, Langmuir 17 (2001) 5025-5030.

[4] C. Burda, Y. Lou, X. Chen, A.C.S. Samia, J. Stout, J.L. Gole, Nano Lett. 3 (2003) 1049-1051.

[5] M. Sathish, B. Viswanathan, R.P. Viswanath, C.S. Gopinath, Chem. Mater. 17 (2005) 6349-6353.

[6] T.C. Jagadale, S.P. Takale, R.S. Sonawane, H.M. Joshi, S.I. Patil, B.B. Kale, S.B. Ogale, J. Phys. Chem. C 112 (2008) 14595-14602.

[7] K.A. Michalow, D. Logvinovich, A. Weidenkaff, M. Amberg, G. Fortunato, A. Heel, T. Graule, M. Rekas, Catal. Today 144 (2009) 7-12.

[8] M. Xing, J. Zhang, F. Chen, Appl. Catal. B 89 (2009) 563-569.

[9] D. Chatterjee, S. Dasgupta, J. Photoch. Photobio. C 6 (2005) 186-205.

[10] A. Zaleska, Recent Pat. Eng. 2 (2008) 157-164.

[11] S. Rehman, R. Ullah, A.M. Butt, N.D. Gohar, J. Hazard. Mater. 170 (2009) 560-569.

[12] S. Malato, P. Fernández-Ibáñez, M.I. Maldonado, J. Blanco, W. Gernjak, Catal. Today 147 (2009) 1-59.

[13] C.L. Bianchi, G. Cappelletti, S. Ardizzone, S. Gialanella, A. Naldoni, C. Oliva, C. Pirola, Catal. Today 144 (2009) 31-36.

[14] H. Ichinose, M. Taira, S. Furuta, H. Katsuki, J. Am. Ceram. Soc. 86 (2003) 1605-1608.

[15] Y. Gao, Y. Masuda, Z. Peng, T. Yonezawa, K. Koumoto, J. Mater. Chem. 13 (2003) 608-613.

[16] Y. Gao, Y. Masuda, W.-S. Seo, H. Ohta, K. Koumoto, Ceram. Int. 30 (2004) 1365-1368.

[17] B. Ohtani, Y. Azuma, D. Li, T. Ihara, R. Abe, Trans. Mater. Res. Soc. Jpn. 32 (2007) 401-404.

[18] D.-E. Gu, B.-C. Yang, Y.-D. Hu, Catal. Commun. 9 (2008) 1472-1476.

[19] A. Kubacka, B. Bachiller-Baeza, G. Colón, M. Fernández-García, Appl. Catal. B: 93 (2010) 274-281.

[20] I. El Saliby, L. Erdei, H.K. Shon, J.-H. Kim, J. Ind. Eng. Chem. 17 (2011) 358-363.

[21] S. Senthilkumaar, K. Porkodi, J. Colloid Interf. Sci. 288 (2005) 184-189.

[22] H.W. Chen, Y. Ku, Y.L. Kuo, Chem. Eng. Technol. 30 (2007) 1242-1247.

[23] L. Liu, Z. Liu, H. Bai, D.D. Sun, Water Res. 46 (2012) 1101-1112.

[24] H. Bai, Z. Liu, D.D. Sun, Chem. Asian J. 7 (2012) 1772-1780.

[25] J.H. Pan, X. Zhang, A.J. Du, D.D. Sun, J.O. Leckie, J. Am. Chem. Soc. 130 (2008) 11256-11257.

[26] K.S.W. Sing, D.H. Everett, R.A.W. Haul, L. Moscou, R.A. Pierotti, J. Rouquerol, T. Siemieniewska, Pure. Appl. Chem. 57 (1985) 603-619.

[27] S. Sato, R. Nakamura, S. Abe, Appl. Catal. A 284 (2005) 131-137.

[28] A.V. Emeline, V.N. Kuznetsov, V.K. Rybchuk, N. Serpone, Int. J. Photoenergy Volume 2008, Article ID 258394, 19 pages.

[29] D. Lützenkirchen-Hecht, H.-H. Strehblow, Surf. Interface. Anal. 41 (2009) 820-829.

[30] C.Q. Sun, Prog. Solid. State. Ch. 35 (2007) 1-159.

[31] C.-C. Chen, H.-J. Fan, C.-Y. Jang, J.-L. Jan, H.-D. Lin, C.-S. Lu, J Photochem. Photobio. A 184 (2006) 147-154.

[32] A.d.O. Martins, V.M. Canalli, C.M.N. Azevedo, M. Pires, Dyes Pigments 68 (2006) 227-234.

Tables

Table 1

Structural parameters of nitrogen doped and silver co-doped photocatalysts

Photocatalyst	$S_{BET}{}^{a}$ (m^2/g)	$V_p{}^{b}$ ($cm^3\ g^{-1}$)	$D_p{}^{c}$ (Å)
TiN	52.47	0.23	46.30
TiNAg	52.91	0.31	60.87

[a] BET surface area

[b] Total mesopore volume

[c] Mean mesopore diameter as estimated from nitrogen desorption isotherms using the Barrett-Joyner-Halenda (BJH) model

Table 2

Chemical composition of photocatalysts obtained from XPS elemental analysis

Sample	Ti (at.%)	O (at.%)	N (at.%)	Ag (at.%)
TiN	36.69	55.24	1.38	-
TiNAg	38.78	56.37	1.46	0.15-0.2

List of Figures

Figure 1. Scheme describing different steps in TiN and TiNAg synthesis.

Figure 2. SEM micrographs of prepared photocatalysts.

Figure 3. TEM images of TiN and TiNAg.

Figure 4. XRD diffraction patterns of TiN and TiNAg.

Figure 5. Nitrogen adsorption/desorption isotherms of TiN and TiNAg.

Figure 6. DRS spectra of TiN and TiNAg.

Figure 7. XPS spectra for the N 1s region of TiN and TiNAg and the Ag 3d region of TiNAg.

Figure 8. Photocatalytic discolouration and DOC removal of CV solution using TiN and TiNAg under simulated solar light ([CV] = 10 mg/L, Catalyst loading = 1 g/L, T = 26°C, air sparging = 0.6 L/min, pH = 6.2, sampling done every 30 min).

Figure 1

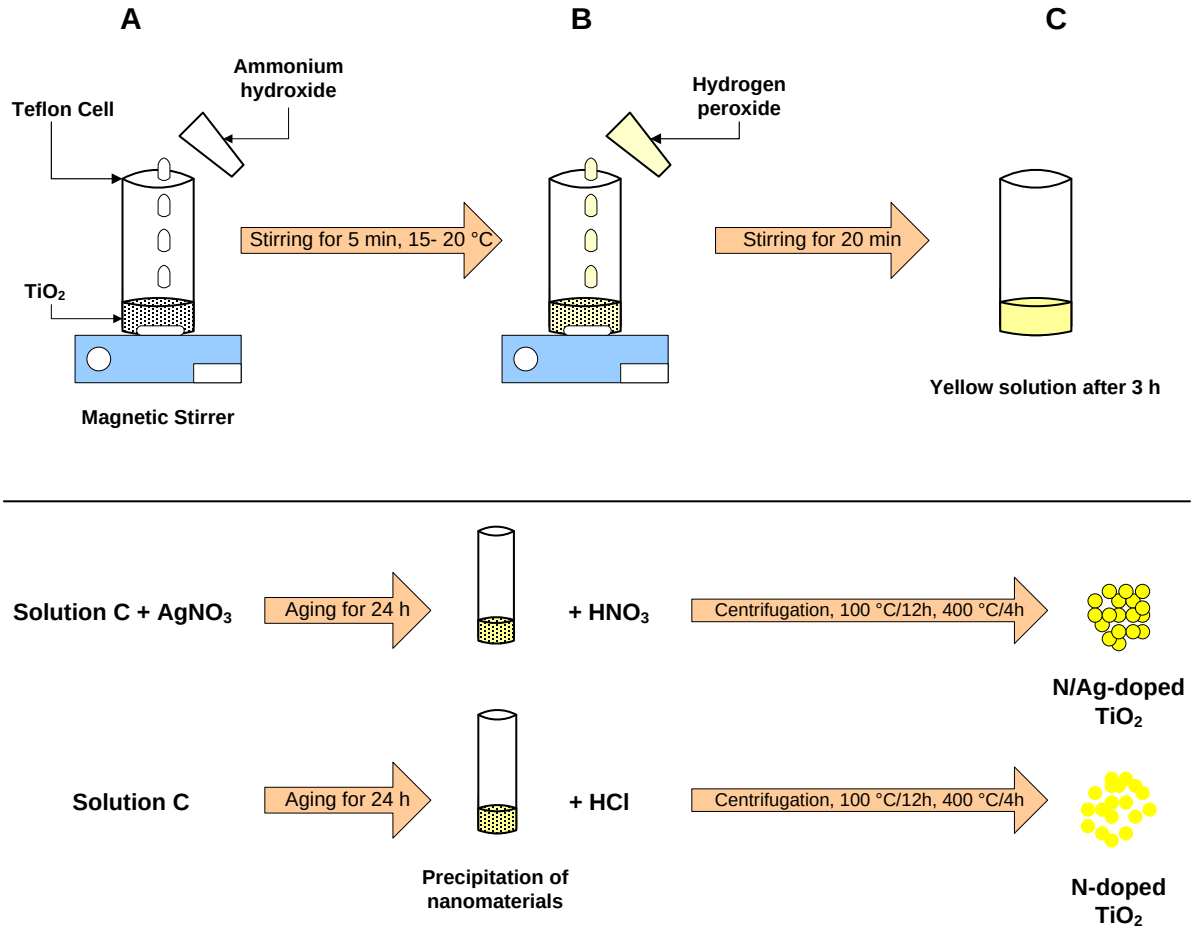
A
B
C
Ammonium hydroxide
Teflon Cell
Hydrogen peroxide
Stirring for 5 min, 15- 20 °C
Stirring for 20 min
TiO2
Magnetic Stirrer
Yellow solution after 3 h
Solution C + AgNO3
Aging for 24 h
+ HNO3
Centrifugation, 100 °C/12h, 400 °C/4h
N/Ag-doped TiO2
Solution C
Aging for 24 h
+ HCl
Centrifugation, 100 °C/12h, 400 °C/4h
Precipitation of nanomaterials
N-doped TiO2

Figure 2

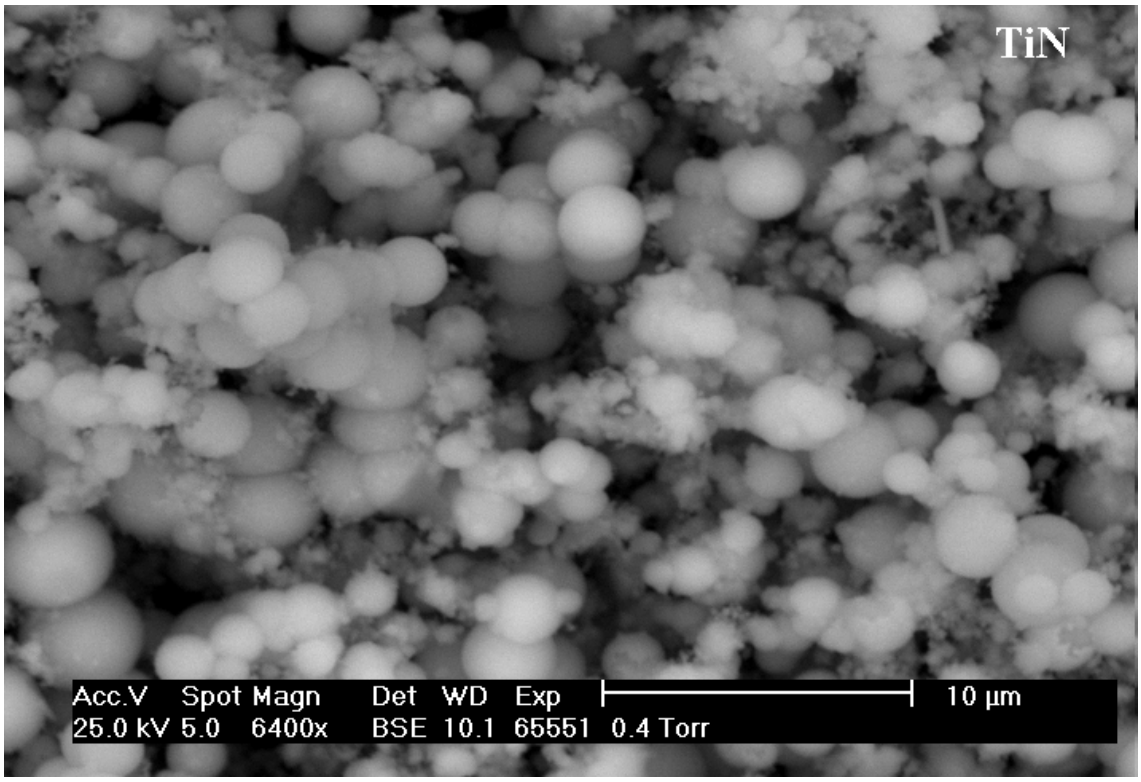
TiN
Acc.V Spot Magn Det WD Exp
10 µm
25.0 kV 5.0 6400x BSE 10.1 65551 0.4 Torr

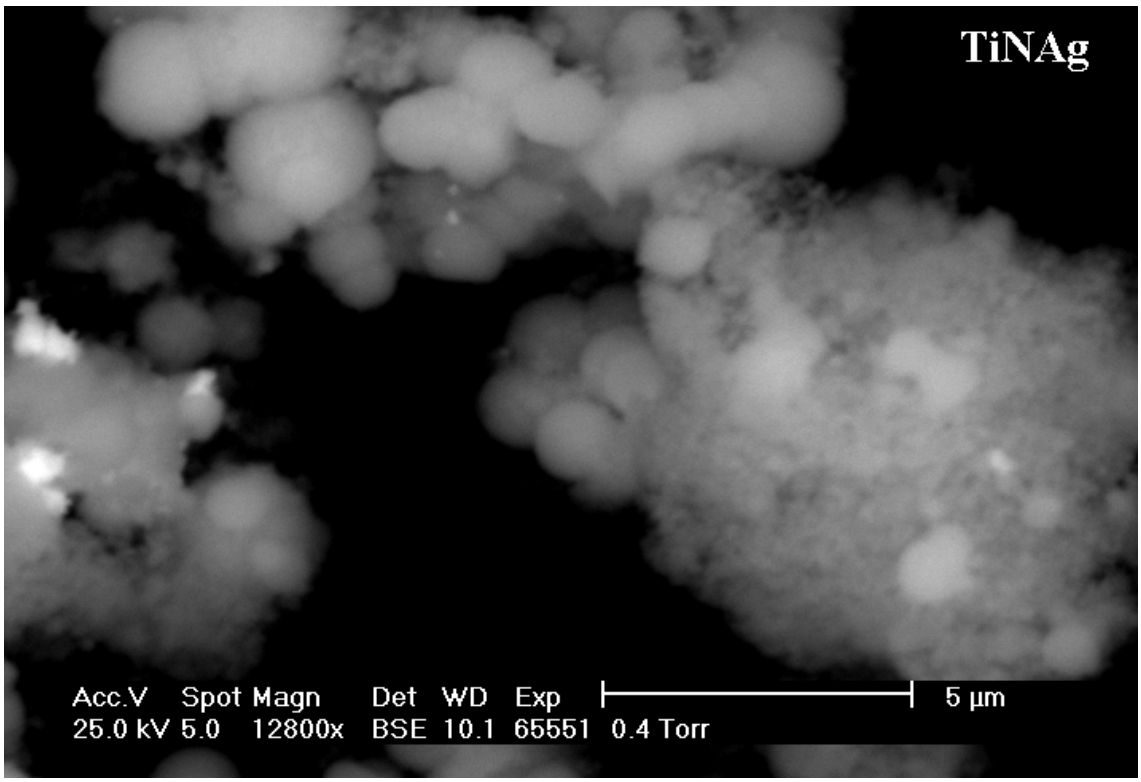
TiNAg
Acc.V Spot Magn Det WD Exp
5 µm
25.0 kV 5.0 12800x BSE 10.1 65551 0.4 Torr

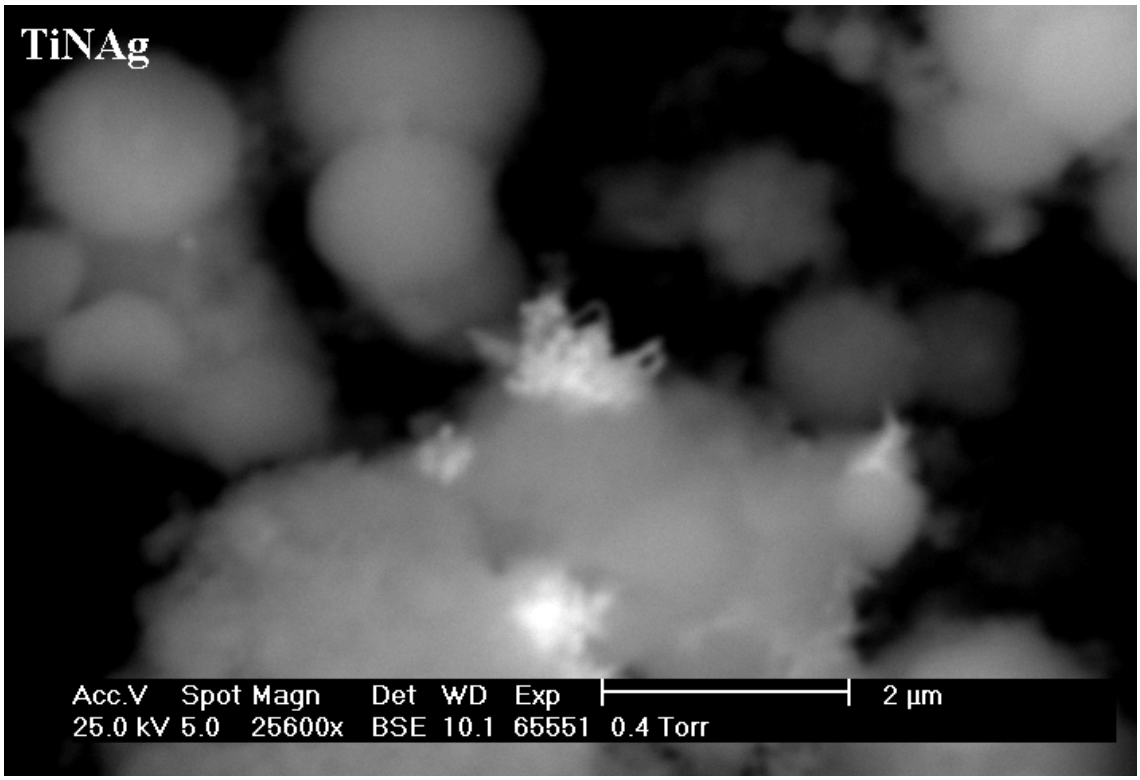
TiNAg
Acc.V Spot Magn Det WD Exp
2 µm
25.0 kV 5.0 25600x BSE 10.1 65551 0.4 Torr

Figure 3

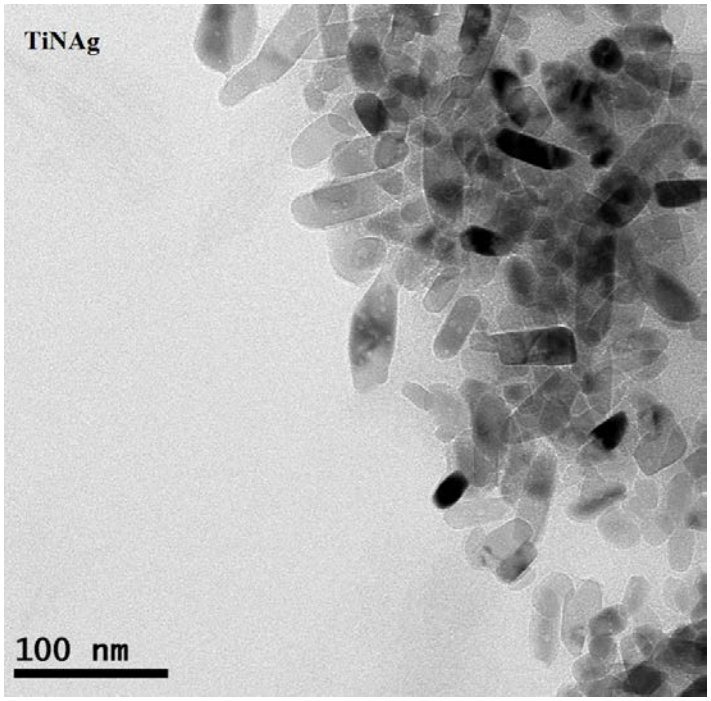

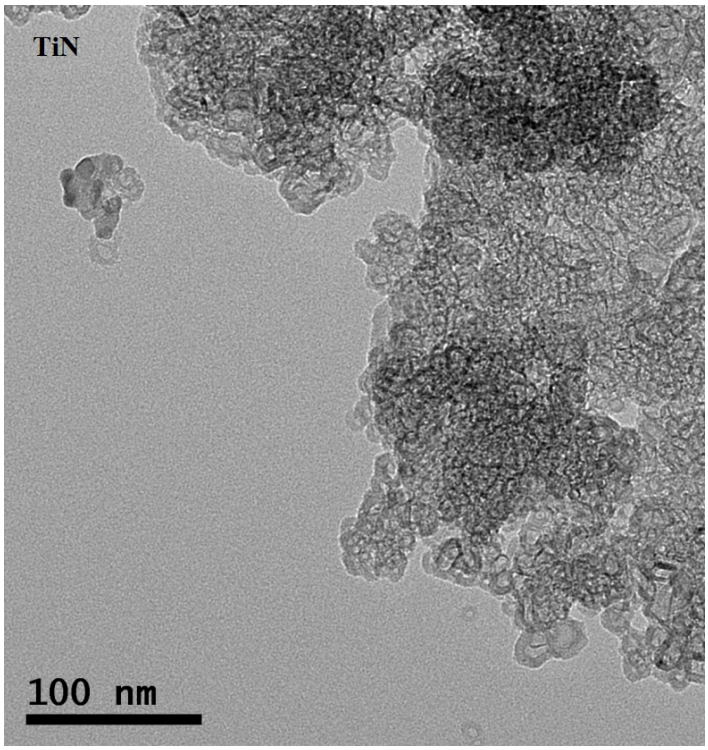

Figure 4

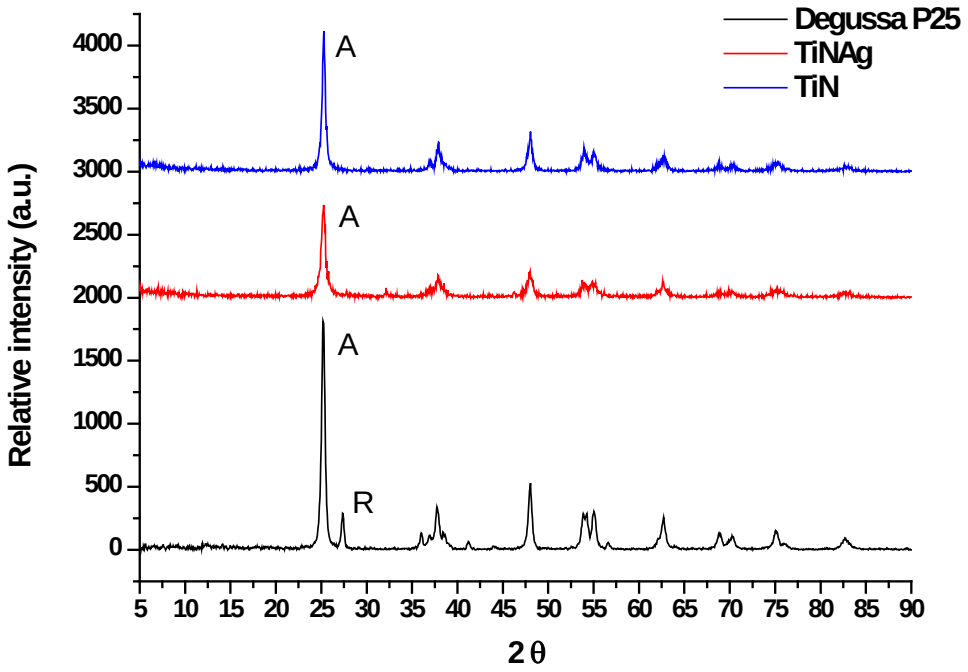
Degussa P25
TiNAg
TiN
A
A
A
R
Relative intensity (a.u.)
4000
3500
3000
2500
2000
1500
1000
500
0
5
10
15
20
25
30
35
40
45
50
55
60
65
70
75
80
85
90
2θ

Figure 5

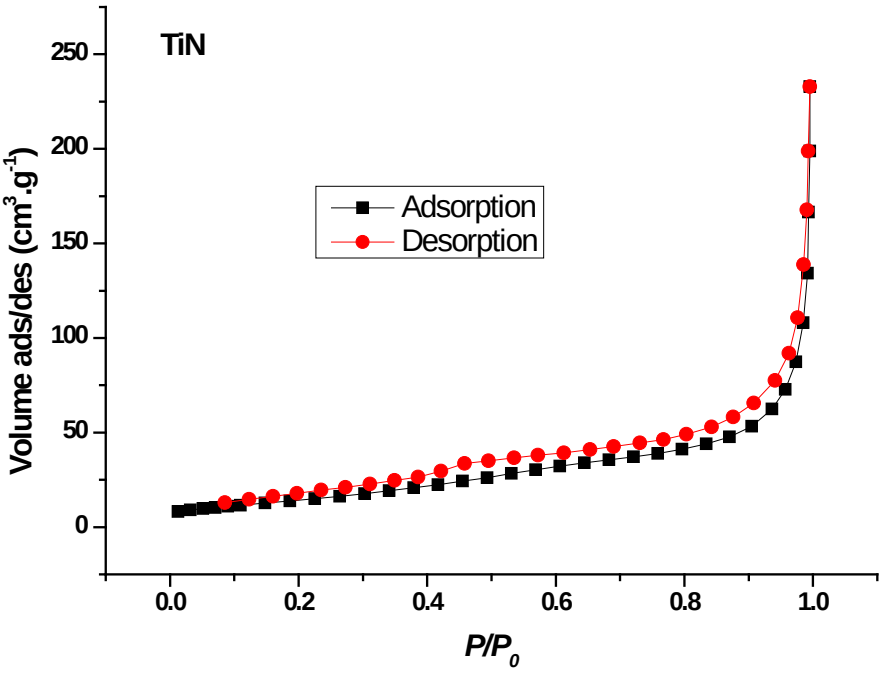
TiN
Adsorption
Desorption
Volume ads/des (cm3.g-1)
P/P0
0
50
100
150
200
250
0.0
0.2
0.4
0.6
0.8
1.0

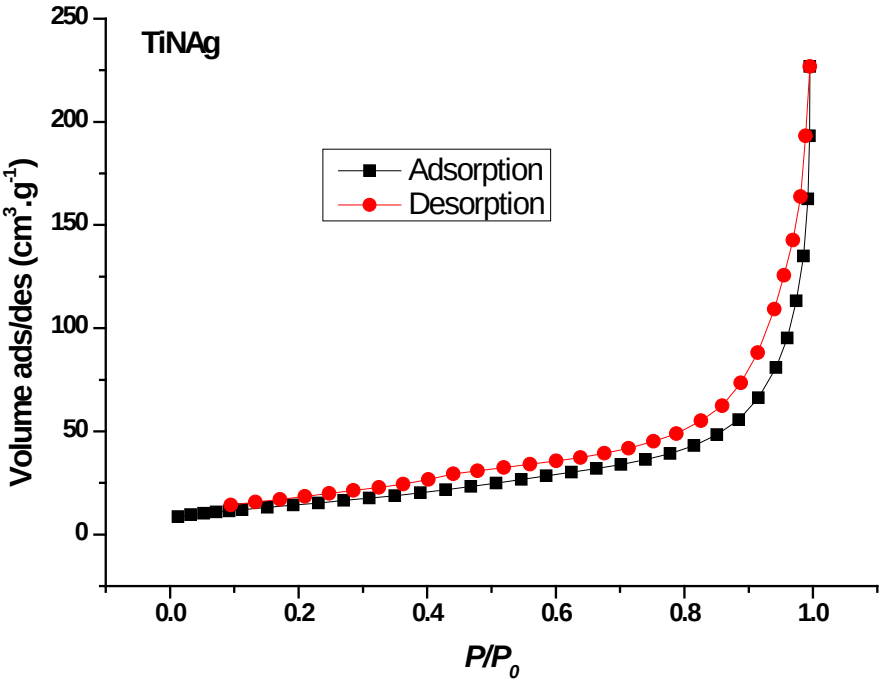
TiNAg
Adsorption
Desorption
Volume ads/des (cm3.g-1)
P/P0
0
50
100
150
200
250
0.0
0.2
0.4
0.6
0.8
1.0

Figure 6

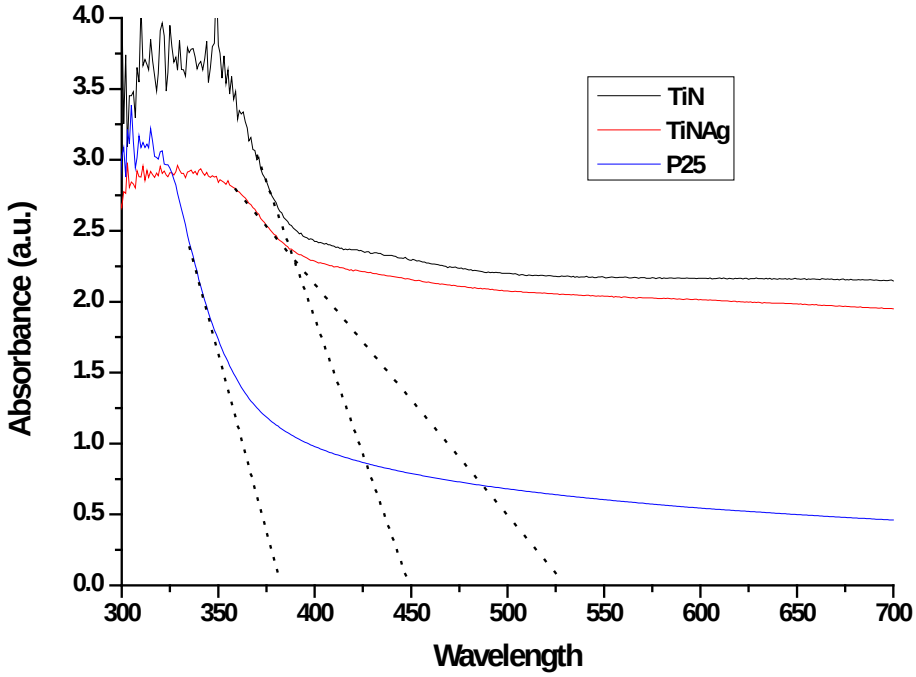
Absorbance (a.u.)
Wavelength
TiN
TiNAg
P25
4.0
3.5
3.0
2.5
2.0
1.5
1.0
0.5
0.0
300
350
400
450
500
550
600
650
700

Figure 7

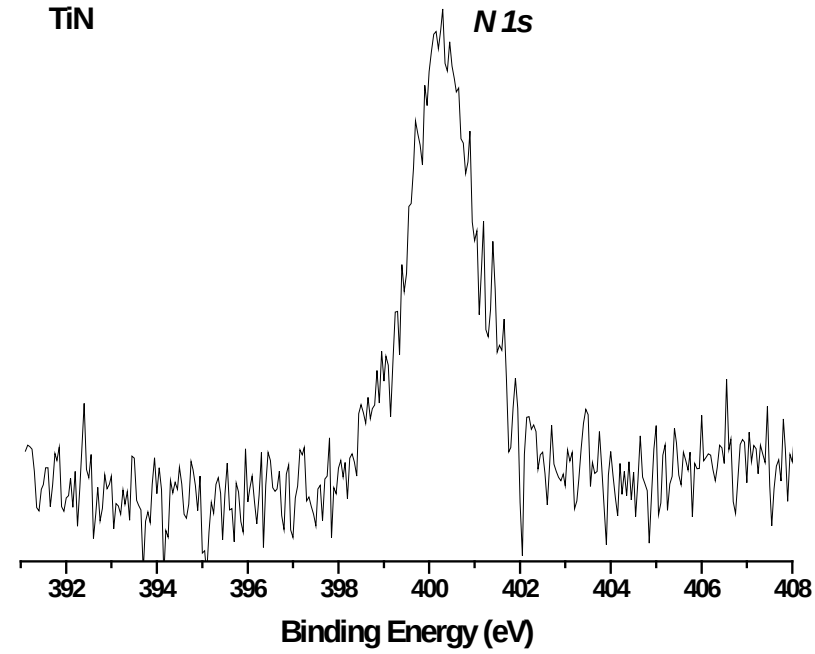
TiN
N 1s
392
394
396
398
400
402
404
406
408
Binding Energy (eV)

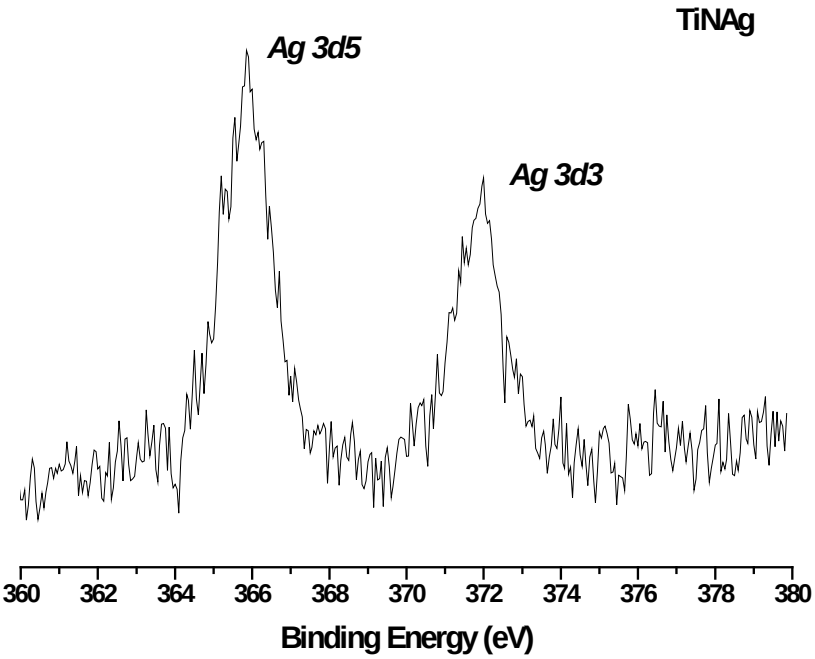
TiNAg
Ag 3d5
Ag 3d3
360
362
364
366
368
370
372
374
376
378
380
Binding Energy (eV)

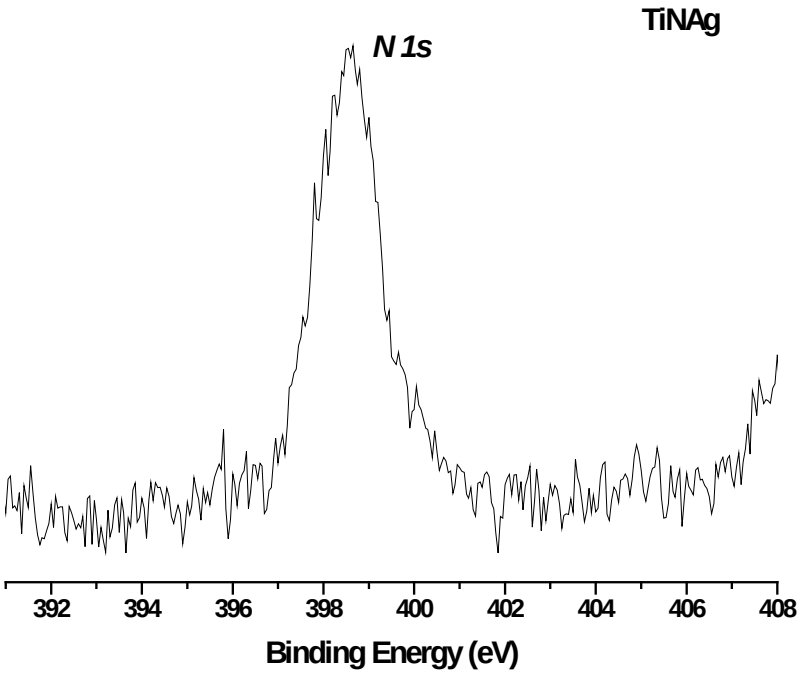
TiNAg
N 1s
392
394
396
398
400
402
404
406
408
Binding Energy (eV)

Figure 8

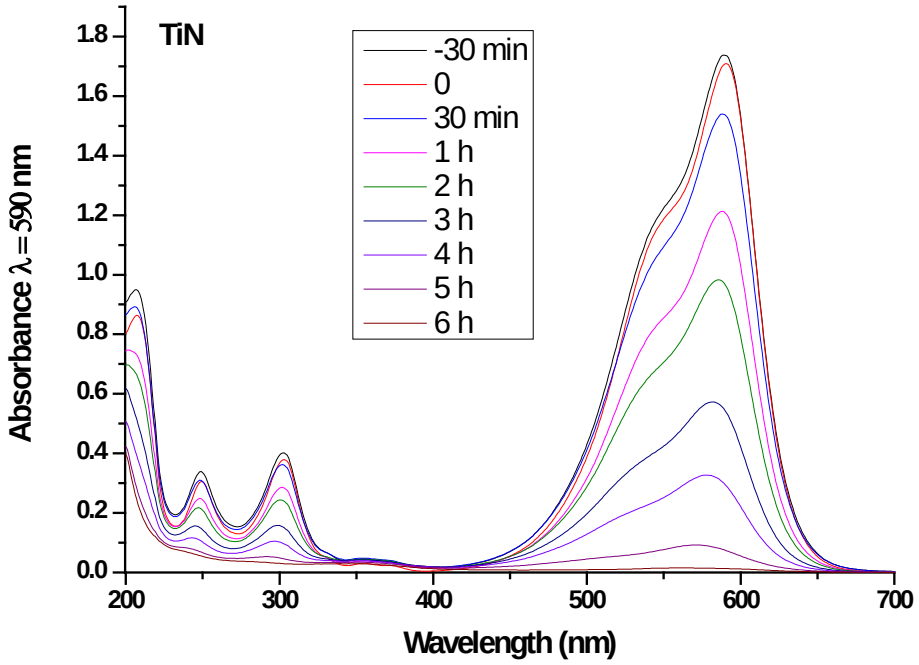
TiN
-30 min
0
30 min
1 h
2 h
3 h
4 h
5 h
6 h
Absorbance λ = 590 nm
Wavelength (nm)

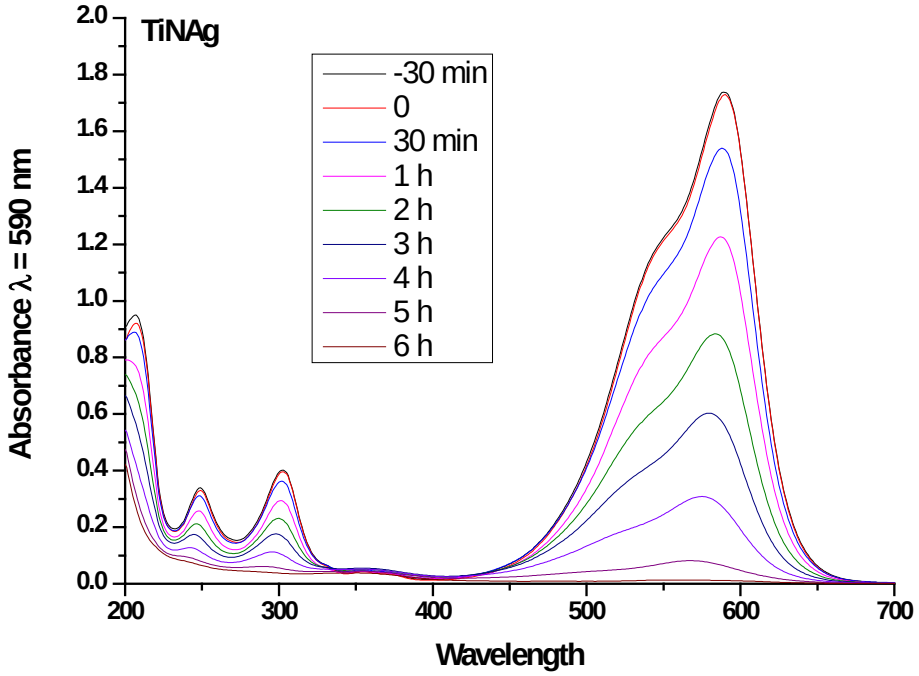
TiNAg
-30 min
0
30 min
1 h
2 h
3 h
4 h
5 h
6 h
Absorbance λ = 590 nm
Wavelength

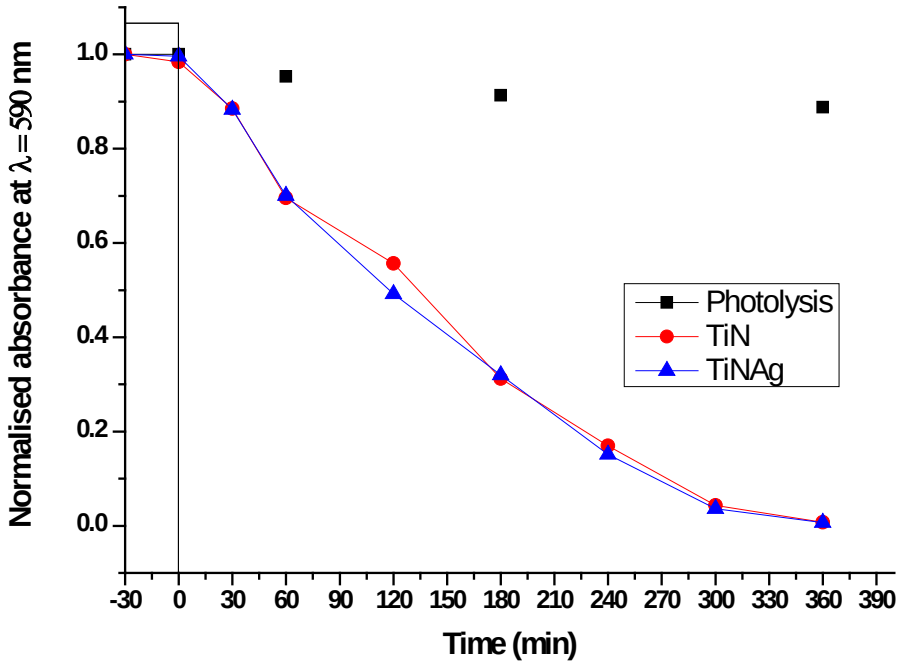
Normalised absorbance at λ = 590 nm
1.0
0.8
0.6
0.4
0.2
0.0
-30
0
30
60
90
120
150
180
210
240
270
300
330
360
390
Time (min)
Photolysis
TiN
TiNAg

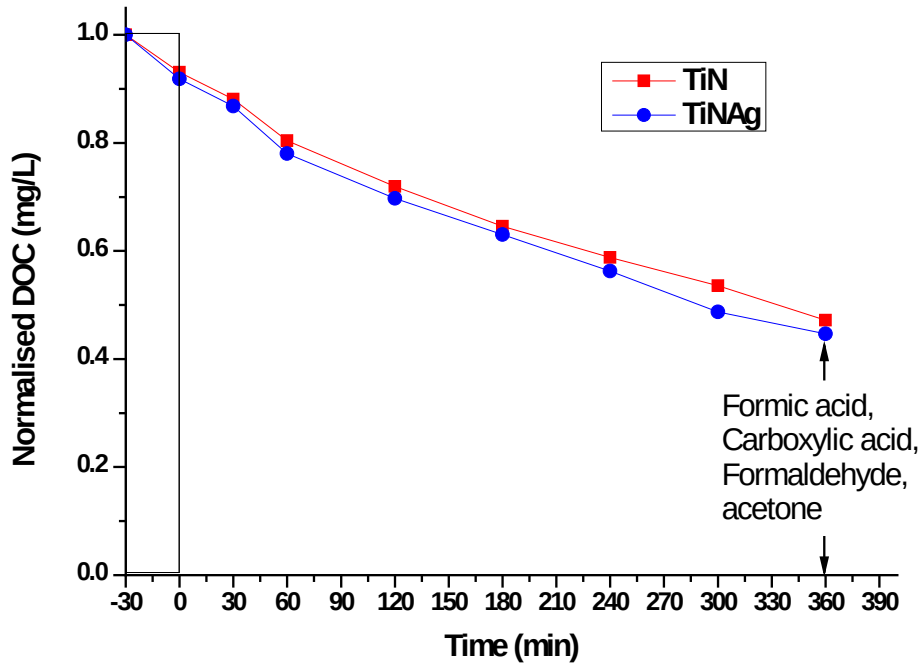
Normalised DOC (mg/L)
1.0
0.8
0.6
0.4
0.2
0.0
-30
0
30
60
90
120
150
180
210
240
270
300
330
360
390
Time (min)
TiN
TiNAg
Formic acid,
Carboxylic acid,
Formaldehyde,
acetone